HIGH PRESSURE VAPOR TRANSPORT OF BINARY AND TERNARY COMPOUND SEMICONDUCTORS

S. Fiechter* , R. H. Castleberry, G. Wood and K. J. Bachmann
and
H. T. Tran, K. Ito and J. S. Scroggs
Department of Materials Science and Engineering
and
Department of Mathematics
North Carolina State University, Raleigh, North Carolina
27695-7919

Abstract

Crystals of II-IV-V_2 chalcopyrite $ZnGeP_2$ (E_g = 2.34 eV) and of III-V zincblende InP (E_g = 1.27 eV) have been grown by High Pressure Vapor Transport (HPVT) in evacuated and sealed quartz glass ampoules. Semiconductor melts were used as source material and an addition of phosphorus suppressed thermal decomposition of the melt. Thermochemical equilibrium calculations reveal that the equilibrium vapor phase over $ZnGeP_2$ at the melting point T_m=1295 K contains 81.9 mol% P_4, 11.3 mol% P_2, 6.8 mol% Zn, but only $3 \cdot 10^{-10}$ mol% Ge. The vapor phase over InP (T_m=1335 K) consists of 94.2 mol% P_4, 5.8 mol% P_2 and $6.8 \cdot 10^{-6}$ mol% In. In spite of the extremely low Ge partial pressure, high $ZnGeP_2$-transport rate is observed, relating to a flux of $5 \cdot 10^{-6}$ mole /m^2s at 1295 K and 1g. Contributing factors to this unexpectedly high flux are the formation of volatile molecular Ge-species (e.g. GeO and GeP) and a strong convective flow that is mainly driven by a pronounced pressure/temperature drop (67 mbar/K) for transport close to the melting point. This behaviour is even more pronounced growing InP by HPVT. Numerical solutions to the Navier-Stokes equation in a Scholz geometry fused silica vessel for the boundary conditions of HPVT revealed that at µg only two vortices exist; one above and one below the ring-shaped source trough achieving optimum mixing and transport to the substrate. Formation of additional vortices and an increase of the flow velocity occurs as the gravity factor increases from µg to 1g. Thus, reduced gravity is conducive to the control of HPVT crystal growth.

I. Introduction

At liquidus temperatures in the vicinity of the melting temperatures, InP and $ZnGeP_2$ exhibit high dissociation pressures, which sensitively change with the composition of the solidus in equilibrium [1, 2]. Over the stoichiometric melts they are 27.5 and 3.5 bars, respectivly. Therefore, the control of the partial pressures of the constituents during high vapor pressure transport (HPVT) provides for the close control of the stoichiometry of the growing crystal. For example, using the melt of the compounds as source for vapor phase growth, $ZnGeP_2$ crystals of higher transparency can be achieved [3, 4] than those grown from the melt.

InP and $ZnGeP_2$ crystallize in the zincblende and the chalcopyrite structure, respectively and have remarkable optoelectronic properties [5 - 7]. InP is an important substrate material for the fabrication of light sources and detectors operating in the near infrared wavelength region, where silica-based optical fibers exhibit minimum dispersion and loss. Its favorable surface properties permit the construction of FET circuits with high channel mobility and low density of interface states. Unfortunately, the fabrication of nominally undoped semi-insulating InP remains elusive due to the relatively shallow energy of the P_{In} antisites and the difficulty in controlling the concentration of native point defects in this material. $ZnGeP_2$ possesses the largest effective nonlinear optical susceptibility tensor component (d_{eff} = 75×10^{12}m/volt) of any semiconductor that is transparent in the 2 to 12µ range [8]. This property, coupled with a large birefringence due to the axial compression of the unit cell along the c-axis, makes this material ideal for frequency mixing applications such as second harmonic generation (SHG) and for use in optical parametric oscillators.

The present paper discusses the thermochemical properties of both materials taking into account all thermodynamical data available and comparing experimental results with thermochemical equilibrium calculations using the method described by Ericson [9].

These calculations allow a prediction of the composition and the densities of the vapor phase, of which all are needed as input data for modeling the gas flow dynamics and heat transfer of HPVT under both ground based and microravity conditions. Other data such as viscosity and binary diffusion coefficients, rate constants and activation energies of the gas reactions must be calculated separately. This paper compares the contributions of convective flow and diffusion controlled transport to the observed transport rates.

*permanent address: Hahn-Meitner-Institut,
Department of Physical Chemistry,
Glienicker Str. 100, D-14109 Berlin, Germany

6th International Symposium on
Experimental Methods for Microgravity Materials Science
Edited by Robert A. Schiffman and J. Barry Andrews
The Minerals, Metals & Materials Society, 1994

II. Thermal stability and equilibrium vapor phases above InP and $ZnGeP_2$

Heating InP or $ZnGeP_2$ in an evacuated, closed system causes thermal decomposition of the material. The decompositon reactions close to the melting point are due to ref. [1]:

$$InP(l) \leftrightarrow In(l) + 1/4\ P_4(g) \quad (1.1)$$
$$In(l) \leftrightarrow In(g) \quad (1.2)$$
$$P_4(g) \leftrightarrow 2\ P_2(g) \quad (1.3)$$

and those of $ZnGeP_2$ as a result of the below described thermochemical calculations:

$$ZnGeP_2(s) \leftrightarrow 1/3 Zn_3P_2(s) + Ge(l) + 1/3 P_4(g) \quad (2.1)$$
$$Zn_3P_2(s) \leftrightarrow 3\ Zn(g) + 1/2\ P_4(g) \quad (2.2)$$
$$P_4(g) \leftrightarrow 2\ P_2(g) \quad (2.3)$$
$$Ge(l) \leftrightarrow Ge(g) \quad (2.4)$$

The total pressure vs. temperature equations reported in the literature or inferred from vapor pressure data are
a) for InP [1]:

$$\log p\ (bar) = 26.520 - 33839/T \quad (3.1)$$
$$\Delta T = 1250\text{-}1326K$$

$$\log p\ (bar) = 67.098 - 87645/T \quad (3.2)$$
$$\Delta T = 1326\text{-}1335K$$

b) for $ZnGeP_2$ [2]:

$$\log p\ (bar) = 17.172 - 21466/T \quad (4)$$
$$\Delta T = 1240\text{-}1295K$$

and
c) for the important dissociation product Zn_3P_2 [10, 11]:

$$\log p\ (bar) = 6.9293 - 9008/T \quad (5.1)$$
$$\Delta T = 620\text{-}820K$$

$$\log p\ (bar) = 6.1833 - 8377.2/T \quad (5.2)$$
$$\Delta T = 1040\text{-}1390K.$$

To determine the vapor phase composition over the compounds, thermochemical calculations have been performed employing the Gibbs free energy minimization technique via the program Chemsage [9]. For this purpose, the thermochemical data of all solid, liquid and gaseous species have to be known, i.e. heats of formation, standard entropies, molar heats and their temperature dependence. The data used for these quantities are summarized in table I(a). Unfortunately, the experimentally determined heat of formation values can exhibit large errors. In order to conduct the calculations as close as possible to experimentally observed pressure measurements and phase equilibria, the heat of formation of the condensed phases were modified using a recursive procedure which was performed for all subsystems. Because of limited experimental data in some cases (e.g. for the vapor phase over GeP) or contrary results in the literature, the question arose whether this procedure leads to unambiguous input parameters. The question has been intensively exercised for $ZnGeP_2$ where up to three condensed phases can be in equilibrium with the vapor phase at the melting point under certain P-T-x conditions. Under the assumption that the considered chalcopyrite has a melting point at T_m = 1295 K and an equilibrium pressure in the range from 3.5-3.9 bar [2,12], only one enthalpy-of-formation parameter-set was found to fit the experimental findings. The standard heat of formation values and, in the case of phosphorus, the P(red)-P_4(white) phase transition energy were slightly changed to emulate the experimentally determined pressures at the melting points of the element P [1], of the binary compounds InP [1], ZnP_2 [18], Zn_3P_2 [10] and GeP [14] as well as of the ternary $ZnGeP_2$ [2]. In table I(b) the adapted values are compared with data, reported in the literature.

III. HPVT-experiments

High Pressure Vapour Transport (HPVT) experiments have been conducted for $ZnGeP_2$ in a modified Scholz geometry ampoule (figure 1), and in conventional horizontal quartz tubes. The HPVT furnace for the Scholz geometry is comprised of three heating (h_1-h_3) and two cooling zones (the top plug P and the bottom fused silica window W). The temperature distribution in the ampoule under growth conditions is $T_1 < T_2 > T_3$ and $T_1 > T_3$. This configuration was chosen since transport in endergonic reactions proceeds from hot to cold which applies to HPVT of $ZnGeP_2$ and InP. The $ZnGeP_2$ source material is thus transported from S to G. In the horizontal experiment a two zone furnace with a glow bar in the middle to provide a thermal spike as well as a single zone furnace were utilized to study the transport behaviour under different conditions.

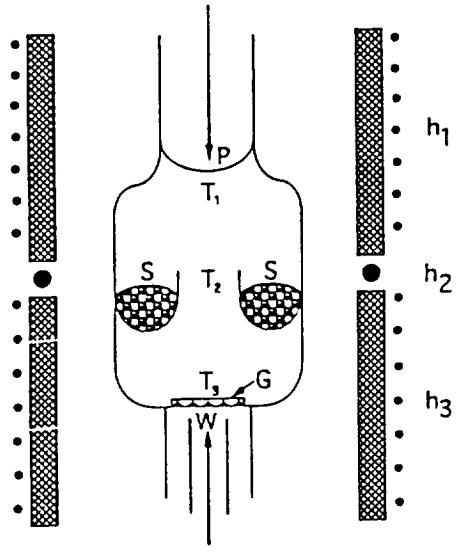

Figure 1: Schematic representation of the Scholz-type geometry ampoule for HPVT of $ZnGeP_2$ filled with a $Zn/P_2/P_4$ vapor of 3.5 bar pressure at 1295 K. h_1-h_3 are independently controlled heaters; P and W are locations of heat extraction by gas jets impinging onto the outside of the capsule.

Table I(a) Thermochemical data used for free energy minimization calculations due to refs. 2 and 13. For adjusted data see table I(b). The dimensions of the standard heat of formation ΔH_f^o, heat of fusion ΔH_{fu} or heat of evaporation ΔH_e are kcal/mole. For the standard entropies S_f and molar heats c_p, the units are cal/mole deg.

Element/ Compound	ΔH_f^o ΔH_{fu} ΔH_e	S_f^o	$c_p = A+B\cdot10^{-3}\cdot T+C\cdot10^5\cdot T^{-2}$ A	B	C	
Zn(s)	0.00	9.943	5.096	2.782	0.13	
Zn(l)	1.75		7.495			
Zn(g)	31.15	38.451	4.965			
In(s)	0.00	13.81	2.618	9 517	-0.8287	
In(l)	0.779		7.135	-0.2128		T>430 K
In(l)	0.00		6.94			T>900 K
In(g)	58.84	41.50	5.418	0.5646	-0.5684	
Ge(s)	0.00	7.425	5.577	0.931	-0.25	
Ge(l)	8.82		6.596			T>1210 K
Ge(g)	89.34	40.1	7.038	-0.873	0.76	
P(red)	0.00	5.45	4.051	3.559		
P4(white)	16.68	39.28	18.28	15.12		
P(l)	17.31		25.168			T>317 K
P4(g)	30.77	66.89	19.562	0.162	-3.213	
P2(g)	40.68	52.11	8.675	0.191	-0.994	
GeP(s)	-0.13	14.6	10.84	2.7	-1.25	
InP(s)	-11.16	14.28	9.79	3.497		
InP(s)	0.09		13.190			T>910 K
InP(l)	15.		14.0			T>1335 K
$ZnGeP_2$	-26.3	28.22	24.65	3.5	-4.0	
ZnP_2	-24.15	14.4	17.01	3.997	0.65	
Zn_3P_2	-38.65	36.2	30.15	6.225	-0.36	

Table I(b) Heat of formation of the compounds $ZnGeP_2$, ZnP_2, Zn_3P_2, GeP and InP in kcal/mole (reference state: red phosphorus)

Author	Technique used	Heat of Formation kcal/mole
InP		
Bachmann [1]	B_2O_3-Bourdon Gauge Method (BGM)	-18.7
Sharirov/ Gadzhiev [17]	Calorimetric bomb (CB) CB	-21.0
Sirota[17]	CB	-21.5
Phillips [17]	Dielectric Function	-20.4
Martosudirdjo [17]	Precipitation Calorimeter	-13.5
Pool [17]	Tin Solution Calorimeter	-14.5
Pauling [17]	Electronegativity (EN)	-11.0
Adapted value due to [1]	Free Energy Minimization (FEM)	-11.15
4 P(red) → P_4(white)		
Rodewald [19]	Heat of Evaporation	16.71
Adapted value due to [1]	FEM	16.68
$ZnGeP_2$		
Borshchevskii [2]	B_2O_3-BGM	-17.9
Adapted value due to [2, 12]	FEM	-17.95
GeP		
Knacke [13]	EN	-2.4
Adapted value due to [14]	FEM	-0.15
ZnP_2		
Kubaschewski [15]	Estimation	-24.3
Lazarev [16]	Vapor Pressure Meas.	-22.2
Alikhanyan [16]	Knudsen Effusion Method	-20.4
Alikhanyan [16]	BGM	-23.9
Adapted value due to [18]	FEM	-24.15
Zn_3P_2		
Schoonmaker [11]	Torsion Effusion method	-39.5
Korb [10]	Quartz-BGM	-40.0
Kubaschewski [15]	Estimation	-38.0
Adapted value due to [10]	FEM	-38.65

Sealing the loaded ampoules is performed with an oxygen-hydrogen torch after the interior pressure has been lowered to ~$5 \cdot 10^{-9}$ bar via an ion pump and two sorption pumps. Prior to the sealing, the ampoules were cleaned for > 48hrs in aqua regia, then rinsed with deionized/distilled water and dried in an oven. Also, once the ampoule is evacuated, just before sealing, it is slightly heated to expel any water vapor. For vertical Scholz geometry ampoules the temperatures were fixed at T_1 = 1290K, T_2 = 1300 K and T_3 = 1280 K during

Table II Vapor phase composition at the melting points of InP, β-ZnP_2, β-Zn_3P_2 and $ZnGeP_2$ and of GeP at T = 832 K.

a) $ZnGeP_2$: T_m = 1295K [2, 12]; condensed phases : $ZnGeP_2$, Ge, Zn_3P_2

Gas Species	Density mole/cm^3	Pressure bar
P_4	7.61E-05	2.77E+00
P_2	1.05E-05	3.81E-01
Zn	6.27E-06	2.28E-01
Ge	4.47E-13	1.63E-08
Total	9.29E-05	3.38E+00

b) β-ZnP_2: T_m = 1313 K [18], phosphorus counterpressure p = 19.7 bar; condensed phase: ZnP_2

Gas Species	Density mole/cm^3	Pressure bar
P_4	1.71E-04	1.86E+01
P_2	1.04E-05	1.14E+00
Zn	1.91E-06	2.09E-01
Total	1.83E-04	1.99E+01

c) β-Zn_3P_2: T_m = 1466 K [18]; condensed phase: Zn_3P_2

Gas Species	Density mole/cm^3	Pressure bar
Zn	6.62E-05	2.64E+00
P_2	9.51E-06	3.79E-01
P_4	6.29E-06	2.51E-01
Total	8.20E-05	3.27E+00

d) GeP: T = 832 K [14]; condensed phases: GeP and Ge; peritectic melting point T_p =1010K [27]

Gas Species	Density mole/cm^3	Pressure bar
P_4	1.44E-04	6.14E-01
P_2	1.31E-08	5.58E-04
Ge	1.41E-21	6.00E-17
Total	1.44E-05	0.61E-01

e) InP: T_m = 1335 K [1]; condensed phases: InP and In

Gas Species	Density mole/cm^3	Pressure bar
P_4	4.24E-04	2.61E+01
P_2	2.59E-05	1.59E+00
In	3.07E-09	1.89E-04
Total	4.50E-04	2.77E+01

HPVT. With horizontal ampoule geometries temperature differentials ranging from 30 up to 80 K have been applied. To date, the largest crystals have been obtained in horizontal ampoules, where the $ZnGeP_2$ transport flux was of the order $5 \cdot 10^{-6}$ mole/m^{2}s at 1300K and 1g. Thus far our HPVT work has been limited to self-seeded platelets, which are of n-type conductivity and exhibit a lower residual absorption in the transparency range than $ZnGeP_2$ crystals grown from the melt [3].

IV. Activation energies and rate constants of the reactions $P_4 \leftrightarrow 2P_2$

To take into account the influence of kinetics on the flow dynamics, activation energies and the pre-exponential factors k_m in the Arrhenius equation $k = k_m \cdot e^{-Ea/RT}$ for reactions in the vapor phase and at the solid-gas interface must be known. A very important role in the vapor phase regime plays the P_4/P_2 equilibrium which is expressed by the reactions

$$P_4 \rightarrow 2\,P_2 \qquad (6)$$

and

$$2\,P_2 \rightarrow P_4 \qquad (7)$$

for which the activation energies are unknown. However, from the known reaction enthalpy, ΔH = 53.1 kcal/mole at T = 1295K [13], and the empirical correlation of the activation energies and enthalpies [20], the activation energies for both reactions can be expected to be of the order of 100 cal/mole. Equation (7) can be treated as a bimolecular reaction following the methods of conven-

tional transition state theory applying the equation

$$k_1 = k_B T/h \cdot (q^{\#}/q_a \cdot q_b) \cdot e^{-Ea/RT} \qquad (8)$$

where q_a and q_b relate to the partition functions of the two reactants which are in the case of P_2 identical. $q^{\#}$ is the partition function of the activated P_2-P_2 complex. k_B is the Boltzmann constant, h the Planck constant, E_a the activation energy and R the ideal gas law constant. To determine the partition functions of q_a=q_b and $q^{\#}$, the data used are summarized in table III:

Table III Input parameters [21, 22] and calculated partition functions [20].

Molecule properties	P_2 Molecule	Activated P_2-P_2 Complex
Internuclear distance	1.894 Å	0.78 Å
Vibrational frequency	780.43 cm^{-1}	458 cm^{-1}
Moment of inertia	$9.2 \cdot 10^{-46}$ kgm^2	$1.3 \cdot 10^{-45}$ kgm^2
Partition Functions at 1300 K		
Translational	$4.3 \cdot 10^{33}$ m^{-3}	$1.2 \cdot 10^{34}$ m^{-3}
Rotational	$1.5 \cdot 10^{3}$	$4.1 \cdot 10^{4}$
Vibrational	1.73	2.5

Applying eq. (8), the rate constant for the combination reaction (see eq. 7) is:

$$k_1 = 4.5 \cdot 10^5 \text{ l mole}^{-1} \text{ s}^{-1}.$$

Since the combination reaction is the reverse of unimolecular dissociation, the equilibrium reaction must be the same under all conditions of pressure [20]. At equilibrium the equilibrium constant K_c reads

$$K_c = [P_4]/[P_2]^2 \qquad (9).$$

At high pressures the dissociation is a first order reaction and the rate of dissociation is

$$v_{-1} = k_{-1} \cdot [P_4] \qquad (10.1),$$

the combination reaction is given by

$$v_1 = k_1 \cdot [P_2]^2 \qquad (10.2).$$

From the equations (9) and (10) the rate constant for the unimolecular dissociation at 1295 K was calculated as:

$$k_{-1} = 1.4 \cdot 10^2 \text{ l mole}^{-1} \text{ s}^{-1}.$$

V. Modeling of high pressure vapor transport deposition

The model of transport phenomena in the high pressure vapor transport (HPVT) process involves conservation laws for mass, momentum, energy, and species balance with corresponding boundary conditions. A generalized form of the Navier-Stokes equation for laminar flow and a Newtonian fluid is used to describe momentum conservation. The forms of these equations may be found in standard fluid dynamics texts [23]. However, the following simplifications on the model were made for our numerical computations. First, since the film growth rate is slow compared to the gas-phase dynamics, the flow is assumed to be a steady, i.e. no time derivatives appeared in the mass, momentum, energy and species balance. Second, the Boussinesq approximation is assumed. That is, the mass balance equation is in an incompressible form and the density enters only in the gravitational term of the momentum equation. It is also assumed that all other fluid properties, such as viscosity, conductivity, and specific heat, are constant and the flow is axi-symmetric.

The above coupled set of equations is solved using the finite-element code FIDAP on a non-uniformed quadrillateral grid. In all calculations, zero-slip boundary conditions were assumed at the walls. Calculations were performed to study the gas flow dynamics and heat transport under the conditions of vertical HPVT and gravity levels of 1/10 g to 1/1000 g (microgravity condition). The results of the numerical modeling give invaluable information concerning the choices that need to be made in the thermal boundary conditions to optimize the vapor transport at the source and to establish uniform flow at the surface of the substrate.

In the case of the Scholz type geometry (see fig. 1) the thermal boundary conditions are controlled by separately controlled heating elements (h_1-h_3) and the extraction of heat by gas jets impinging onto the outside of the fused silica envelope both on the top plug P (Temperature T_1) and on the bottom fused silica window W (temperature T_3) that supports the growing crystal G. The heater h_2 establishes a spike T_s in the temperature at the location of the source S. Two independently controlled resistance heaters (h_1 and h_2) keep the outer portions of the ampoule above and below h_2 at a constant temperature. The substrate is located on the fused silica window W.

Major differences in the calculated flow fields and temperature contours of the 1/10 g and 1/100 g cases are apparent in figure 2. Notice that the flow for the 1/10 g case has a maximum flow rate of 8.8×10^{-3} m/s, as compared to the 1/1000 g case, where the maximum

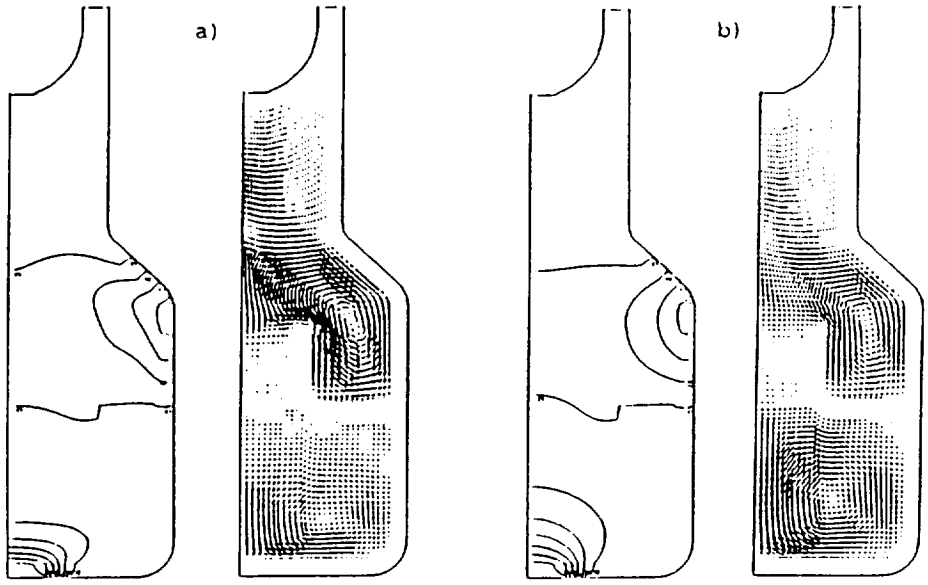

Figure 2: Velocity fields and temperatue contours for the Scholz geometry ampoule, schematically shown in fig. 1, for a) 1/10 g and b) 1/1000 g. The temperatures chosen were T_1 = 1304 K, T_2 = 1317 K and T_3 = 1229 K, the total pressure was 3.5 bar.

flow rate is 1.8 x 10^{-3} m/s. In the plots showing velocity fields, the length of the velocity vectors provides a measure of the relative velocity magnitude. In the 1/10 g case, three recirculation cells occur (Fig. 2.a). These secondary flows are formed due to the density differences between the slower moving fluid along the sidewall and the faster moving and thus less heated fluid along the axis of symmetry and near the substrate. The formation of the convective roll near the top plug could help explain the occurrence of small crystallites observed in that area in our experiments. In the 1/100 g case, two buoyancy driven recirculation cells occur with downward laminar flow directly over the substrate surface (fig. 2.b). Comparison of these cases demonstrate the dramatic effect of gravity on mixed convection flows and temperature contours.
A first order comparison of the contribution from convective flow to the diffusive mass transport at the high pressures and temperatures in the horizontal growth ampoules can be made with the basic equation:

$$\text{Flux}_{\text{convective}} = \text{Density} * \text{Velocity}$$

Diffusive transport was estimated via Schäfer's basic diffusive transport equation [25]. From the work performed by TRAN et. al. [26] an upper limit for the convective flow velocity was obtained at 0.022 m/s. Given the calculated and experimentally measured pressures [2, 12] above the $ZnGeP_2$ and InP melts, the convective flux is expected to be one to two orders of magnitude larger than the diffusive transport contribution.

VI. Discussion

Although the concentrations for Ge and In in the vapor phase are small compared to the concentrations of P_2 and P_4 (see table II.a and e), efficient dissociative sublimation of both $ZnGeP_2$ and InP has been observed for source and substrate temperatures close to the melting points. Under such conditions the interface reaction velocity proceeds quickly compared to the diffusion and convection processes in the gas phase.
Because of the very low Ge concentration calculated to be in the vapor phase, calculated over $ZnGeP_2$ (see table II.a), the question arises, through what mechanism effective transport of $ZnGeP_2$ is achieved.
In the horizontal HPVT experiments, transport rates of 3-4 mg/hr have been observed under a temperature differential ΔT = 1300 - 1270 K over a quartz ampoule with a cross section of $7 \cdot 10^{-4}$ m^2. Estimating the diffusive contribution to the total transport rate, the flux function has been calculated via Schäfer's equation for diffusive transport [24, 25]

$$\Phi_i = D/RT_m \cdot dp_i/dT \Big|_{T_m} \text{grad}_x T \qquad (14),$$

where $\text{grad}_x T = \Delta T/L$ (L= length of the ampoule in m), R = 4.178 $JK^{-1}mole^{-1}$, D is the average binary diffusion coefficient at temperature T_m in m^2/s and dp_i/dT is the pressure temperature slope of gas species i in Pascal. The binary diffusion coefficients have been calculated using the hard sphere model where D_{ij} is given by

$$D_{ij} = 3/8 \cdot (kT/P \cdot \sigma_{ij}^2) \cdot (kT/2\pi\mu_{ij})^{1/2} \qquad (15).$$

P represents the total pressure at temperature T, k is the Boltzmann constant, $\sigma_{ij} = 1/2\ (r_i + r_j)$, where r_i and r_j are the radii of the freely rotating molecules i and j, and μ_{ij} is the reduced mass for the system of the diffusing molecules i and j. The diffusive flux of $ZnGeP_2$, as calculated above, is rate limited by the Ge-concentration and amounts to $2.4 \cdot 10^{-10}$ mole/cm²s. This is about four orders of magnitude smaller than the observed value of $6.5 \cdot 10^{-6}$ mole/cm²s. (The parameters for this calculation were: $D = 4 \cdot 10^{-5}$ m²/s, $dp_{Ge}/dT = 3 \cdot 10^{-2}$g/ms²K, $grad_x T = 30K/3 \cdot 10^{-2}$m).

Convective transport cannot account for the observed transport either (see section V). Therefore, volatile molecular Ge-species must contribute to the transport reaction.
One possible source for the formation of such species is the presence of small amounts of water released from the quartz wall during heating and of oxygen entering by diffusion through the quartz wall into the capsule. This statement is based on an estimate of the oxygen and hydroxyle groups diffusing through 1.125 mm quartz wall of an ampoule with an exterior surface area of 85 cm² which is a typical configuration in our horizontal transport experiments. Using the frequency factor, $D_0 = 2.7 \cdot 10^{-4}$ cm²/s, and the activation energy, $E_a = 1.16$ eV, for oxygen diffusion in quartz [27] the diffusion coefficient at T = 1300K can be calculated to be $8 \cdot 10^{-9}$ cm²/s. Fickian diffusion produces an oxygen concentration of $3.36 \cdot 10^{-7}$ mole/cm³ in the ampoule after 24 hours.
Outgassing of OH^- radicals that are present in type 214 GE quartz tubing and the release of adsorbed H_2O molecules from the interior surface of the ampoule each contribute on the order of 10^{-8} mole/cm³ of oxygen. The sum of these concentrations were introduced as the initial quantity of oxygen in a free energy minimization calculation. The equilibrium vapor phase composition over $ZnGeP_2$ with the addition of the above mentioned quantity of oxygen is markedly different from that given in table II(a). P_4O_6 and GeO are present in the vapor phase with concentrations of $1 \cdot 10^{-7}$ and $3 \cdot 10^{-10}$ mole/cm³ at 1295 K, respectively. They are formed in the reactions

$$2ZnGeP_2(c) + 3O_2(g) \rightarrow P_4O_6(g) + 2Zn(g) + 2Ge(l) \qquad (16.1)$$

$$Ge(l) + 1/3P_4O_6(g) \leftrightarrow GeO(g) + 1/3P_4(g) \qquad (16.2)$$

$$ZnGeP_2(c) + 1/6P_4O_6(g) \leftrightarrow Zn(g) + GeO(g) + 2/3P_4 \qquad (16.3)$$

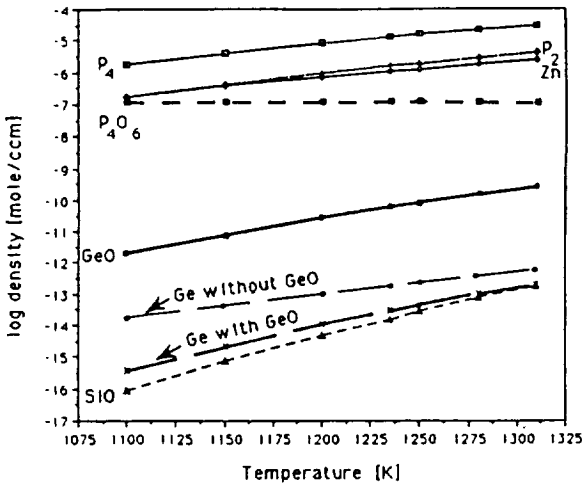

Figure 3: Equilibrium vapor densities above $ZnGeP_2$ vs. temperature introducing O_2 and SiO_2 in the thermochemical calculations (assumed O_2-density: $2.5 \cdot 10^{-6}$ mole/cm³). The doted curve relates to the Ge(g) concentration without oxygen. Thermochemical data for GeO(g) and SiO(g) are taken from ref. [13].

In addition oxygen containing molecular species are formed by the reaction of the vapor phase with the inner wall of the quartz ampoule albeit at an order of magnitude lower concentration than provided by oxygen diffusion (see fig. 3). In the equilibrium calculations both GeO(g) and SiO(g) appear when reaction of the vapor phase with the ampoule is considered. Accordingly, EDX-measurements reveal the incorporation of Si into $ZnGeP_2$ crystals grown by HPVT.
A second source of enhancement to the transport rate are volatile phosphides, e.g. GeP and InP in the vapor phase. To gain the enthalpy and entropy values of these gas species, Pictet-Trouton's rule was applied at the melting points of InP and GeP. Preliminary calculations showed concentrations of the order 10^{-6} mole/cm³.

VII. Concluding remarks

High pressure vapor transport of InP and $ZnGeP_2$ has been discussed on the basis of thermochemical equilibrium calculations, considerations of the kinetics of the reaction $P_2 \leftrightarrow P_4$ and of the experimentally observed transport fluxes. The presence of small amounts of oxygen that enter into the vapor phase by oxygen diffusion and wall reactions results in a significant enhancement of the Ge-concentration in the vapor phase by formation of volatile GeO. The observed InP transport rate is in accord with the equilibrium In-concentration in the gas phase above the melt. Also, convective flow due to the high densities and temperature gradients in the vapor phase enhances the transport rate by 1 to 2 orders of magnitude above the diffusive transport limit. The high phosphorus concentration in the vapor phase also enhances the probability of formation of the gas

species GeP and InP. Reduction of the main source of oxygen by the provision of a pure nitrogen blanket around the growth ampoule and utilization of alternative transport agents such as Cl_2 and HCl are currently being investigated

Acknowledgement

This work was supported by National Aeronautics and Space Administration grant #NAGW-2865.

References

1. K. J. Bachmann, and E. Buehler, "Phase Equilibria and Vapor Pressure of Pure Phoshorus and of the Indium Phophorus System and their Implications Regarding Crystal Growth of InP," J. Electrochem. Soc., 121 (1974), 835-846.

2. A. S. Borshchevskii, and T. M. Shantsovoi, "Pressure and Composition of the Vapor above Semiconductive $ZnGeP_2$," Inorg. Chem., 11 (1975), 1853-1855.

3. G.C. Xing, and K.J. Bachmann , "High-pressure Vapor Transport of $ZnGeP_2$," Appl. Phys. Lett., 56 (1990), 271-273.

4. B. Ray, A.J. Payne, and G.J. Burrell, "Preparation and some Physical Properies of $ZnGeP_2$," phys. stat. sol., 35 (1969), 197-204.

5. a.) G. D. Boyd, W. B. Gandrud, and E. Buehler, " Phase-Matched Up Conversion of 10.6-μ Radiation in $ZnGeP_2$," Appl. Phys. Lett., 18 (1971), 446-448.

b.) G.D. Boyd, E. Buehler, and F.G. Storz, "Linear and Nonlinear Optical Properties of $ZnGeP_2$ and CdSe," Appl. Phys. Lett., 18 (1971), 301-304.

6. Yu.M. Andreev, V.G. Voevodin, P.P. Geiko, A.I. Gribenyukov, V.V. Zuev, A.S. Solodukhin, S.A. Trushin, V.V. Churakov, and S.F. Shubin, "Transformation of the Frequencies of Nontraditional (4.3 and 10.4 μm) CO_2-Laser Radiation Bands in $ZnGeP_2$," Soviet Journal of Quantum Electronics, 17 (1987), 1362-1363.

7. O. Madelung, M. Schulz, and H. Weiss, eds., Landolt-Börnstein, New Series (K.-H. Hellwege, ed.): Crystal and Solid State Physics, vol. III/17a (Springer Verlag, Berlin, 1984), 281-297.

8. J. L. Shay and J. H. Wernick, Ternary Chalcopyrite Structure Semiconductors (Academic Press, New York, 1976), 168.

9. G. Ericson, and K. Hack, "ChemSage - A Computer Program for the Calculation of Complex Chemical Equilibria," Metallurgical Transactions B, 21B (1990), 1013-1023.

10. J. Korb and K. Hein, "Vapor Pressure Investigations in the System Zn-Si-P," (in German), Z. Anorg. Allg. Chem., 425 (1976), 281-288.

11. R. C. Schoonmaker, A. R. Venkitaraman, and F. K. Lee, "The Vaporization of Zinc Phosphide," J. Phys. Chem., 71 (1967), 2676-2683.

12. E. Buehler, and J. H. Wernick, "Concerning Growth of Single Crystals of the II-IV-V Diamond like Compounds $ZnSiP_2$, $CdSiP_2$, $ZnGeP_2$, and $CdSnP_2$ and Standard Enthalpies of Formation for $ZnSiP_2$ and $CdSiP_2$, J. Crystal Growth, 8 (1971), 324-332.

13. O. Knacke, and O. Kubaschewski, Thermochemical Properties of Inorganic Substances (Springer Verlag, Berlin, 1991).

14. M. Zumbusch, M. Heimbrecht, and W. Biltz, "Germanium Phosphide," (in German), Z. Anorg. Allg. Chem., 242 (1939), 237-248.

15. O. Kubaschewski, and C. B. Alcock, Metallurgical Thermochemistry, International Series on Materials Science and Technology, vol. 243 (Pergamon Press, Oxford, 1979), 322.

16. A.S. Alikhanyan, A.V. Steblevskii, Ya.Kh. Grinberg, S.F. Marenkin, C.G. Magomedgadzhiev and V.I. Gorgoraki, "Sublimation of ZnP_2," Inorg.Chem., 14 (1978), 1528-1532 and references therein.

17. S. Martosudirdjo, and J. N. Pratt, "Calorimetric Studies of the Heats of Formation of IIIB-VB Adamantine Phases," Thermochim. Acta, 10 (1974), 23-31 and references therein.

18. J. Berak, and L. Pruchnik, "Phase Equilibria in the Zinc-Cadmium-Phosphorus System. Part II. The Zinc-Phosphorus System," Roczn. Chem. Polon., 43 (1969), 1141-1146.

19. H. J. Rodewald, "The Heat of Transformations of the Phosphorus-Modifications," (in German), Helv. Chim. Acta, 43 (1960), 878-885.

20. Keith J. Laidler, Chemical Kinetics (Harper & Row, Publishers, New York, 1987), 71-74, 89-98 and 171-173.

21. John R. Van Wazer, Phosphorus and its Compounds, vol. I: Chemistry (Interscience Publishers, Inc., New York, 1958), 95-97.

22. N. B. Slater, "Vibrations and Force Constants of Phosphorus," Trans. Faraday Soc., 50 (1954), 207-209.

23. H. Schlichting, Boundary Layer Theory, McGraw-Hill, New York, 1955.

24. H.-U. Finzel, "Transport of Zn_3P_2 by Vapor Phase Transport," (in German), J. Crystal Growth, 50 (1980), 823-830.

25. Harald Schäfer, Chemical Transport Reactions (Academic Press, New York, 1964) 24-25.

26. H. T. Tran, J. S. Scroggs, and K. J. Bachmann, "Modeling of Flow Dynamics and its Impact on the Optimal Reactor Design Problem," in: Identification and Control in Systems Governed by Partial Differential Equations, H. T. Banks, R. F. Fiabiano, K. Ito (eds.), (SIAM Publications, Philadelphia, 1993), 1-3.

26. S. M. Sze, VLSI Technology (McGraw-Hill, New York, 1988), 315.

27.William G. Moffatt, ed., The Handbook of Binary Phase Diagrams, vol. 3 (Genium Publishing Corporation, New York, 1984), 11/82.